# Tunable Yb:KGW laser, CW or Q-switched, enabled by dual-axis tilt of a MOEMS mirror

Alan Paterson, Ralf Bauer, *Member, IEEE*, Walter Lubeigt and Deepak Uttamchandani, *Senior Member, IEEE*

***Abstract*— The experimental proof-of-concept demonstration of an end-pumped Yb:KGW laser with tunable spectral and temporal output characteristics is reported. For the first time, tuning of both of these characteristics in a solid-state laser is achieved simultaneously using a single electrothermally-actuated MOEMS micromirror with controllable tilt angle in two dimensions. In continuous-wave mode, a wavelength tuning range of 22 nm with < 0.3 nm linewidth was achieved by using static MOEMS mirror tilt about one axis to select the intracavity wavelength dispersed by a prism. A wavelength tuning range of 15.3 nm with < 1.1 nm linewidth was achieved in Q-switched operation, by using simultaneous static tilt and resonant scanning of the MOEMS mirror about orthogonal axes. In this operational mode, a pulse repetition rate of 2.06 kHz was obtained with pulse durations varying from 460 ns to 740 ns over the addressable range of laser wavelengths.**

***Index Terms*—Digital laser control, tunable laser, end-pumped Yb:KGW laser, wavelength tuning, active Q-switch, MOEMS, micromirror**

## I. Introduction

ALONGSIDE the benefits of compact design, low-cost batch fabrication and low electrical demands in comparison to their bulk counterparts, the additional benefits of using micro-opto-electro-mechanical systems (MOEMS) in enhancing laser functionality have been demonstrated over a broad range of applications. With multi-kHz scan rates, large scan angles, variable focal length, multi-axis movement mechanisms, or a combination of these features, MOEMS allow innovative routes for optimizing existing laser technology and generating novel laser concepts. Their small footprint and ease of integration with silicon IC-manufacturing provides an ideal approach to produce laser systems with tunable spatial, spectral or temporal output characteristics.

Manuscript submitted November 30, 2017.

A. Paterson acknowledges support from an EPSRC doctoral fund (EP/L505080/1). R. Bauer acknowledges support from the Royal Academy of Engineering under the Engineering for Development Research Fellowship scheme (RF1516\15\8).

A. Paterson was with the Centre for Microsystems and Photonics (CMP), University of Strathclyde (UoS), Glasgow, UK, and is now with Sencio BV, Nijmegen, the Netherlands (alan.paterson.2013@uni.strath.ac.uk).

R. Bauer and D. Uttamchandani are with the CMP, UoS, Glasgow, UK (ralf.bauer@strath.ac.uk, d.uttamchandani@strath.ac.uk).

W. Lubeigt was with the CMP, UoS, Glasgow, UK and is now with M squared lasers, Glasgow, UK (Walter.Lubeigt@m2lasers.com).

Data supporting this research is openly available from http://dx.doi.org/10.15129/a95b3a31-6751-4493-be1f-ab4150214ed5.

Spatial manipulation of laser beams is most commonly performed externally to the lasers [1]. The rapid scan speed and dynamic focal length potential of scanning MOEMS mirrors (also called scanning micromirrors or microscanners), combined with the small device footprint, have been exploited in many applications including pico-projectors [2], barcode readers [3] and biomedical imaging systems [4-6]. As an internal laser component, an adaptive optics mirror enabled by an array of micromachined actuators was reported to compensate for thermal lensing effects in a Nd:$YVO_4$ Raman laser [7].

MOEMS-based tuning of spectral laser characteristics can be achieved by means of either changing the cavity length or by use of dispersive optics. For the case of cavity length changes, the short cavity length of VCSELs results in a small number of longitudinal cavity modes. Using electrostatic potential to displace a MOEMS cantilever or membrane can select the dominant cavity mode, thereby tuning the laser output wavelength [8-10]. Tunable VCSELs have been comprehensively reviewed in literature, e.g. [11]. Alternatively, various configurations involving dispersive optics and MOEMS have been reported to enable wavelength tuning of edge-emitting lasers [12]. A well-known example is the Littman-Metcalf configuration [13-15]. The external-cavity formed by a diffraction grating and a pivoted MOEMS mirror has been reported to enable tunable wavelength ranges of up to 65 nm [16]. Temporal tuning in the form of Q-switching has also been demonstrated in a Nd:$YVO_4$ microchip laser through resonant deformation of a MOEMS mirror using a piezoelectric actuator [17].

In recent years, MOEMS have also been utilized in fiber lasers. Spectral tuning of a continuous-wave (CW) fiber ring laser (35 nm range) was reported using an intracavity MOEMS Fabry-Perot filter [18]. A CW linear-cavity fiber laser (30 nm range) using a digital micromirror array combined with a distributed Bragg reflector has also been reported [19]. Active Q-switching has been reported in fiber lasers using intracavity MOEMS mirrors [20], cantilevers [21-23] and membranes [24-26]. Amongst those was a novel technique to temporally synchronize and spectrally combine multiple MOEMS Q-switched fiber lasers, enabling power-scaling and higher pulse repetition rate [22].

In previous work, we have reported intracavity scanning MOEMS mirrors for active Q-switching of Nd:YLF and Nd:YAG solid-state lasers [27-28], and also a novel technique

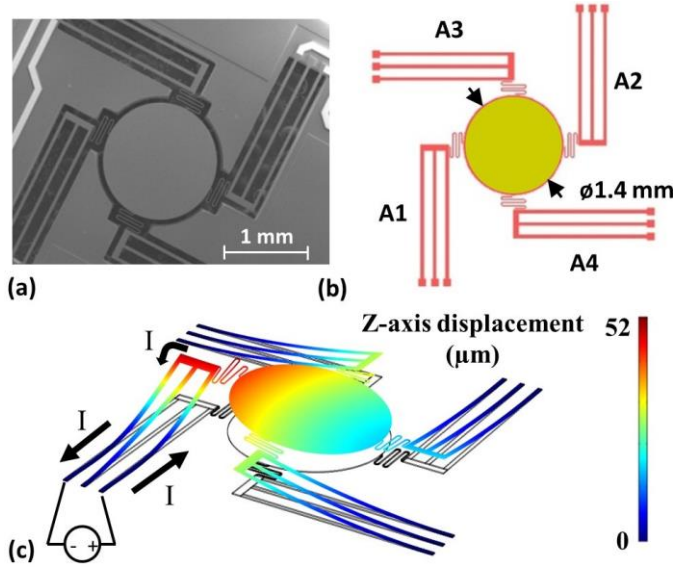


Figure 1: (a) Scanning electron microscope image of the fabricated MOEMS mirror, (b) Diagram of the SCS layer structure (red), a post-fabrication gold coating on the mirror aperture (gold) and labelled actuators from A1 to A4, and (c) Simulated mirror displacement for 7 $V_{dc}$ applied to one actuator.

where a compact MOEMS mirror array enabled two individually Q-switched laser output beams simultaneously originating from one Nd:YAG medium [29]. Recently, a power-scaled, MOEMS Q-switched Er/YB:Glass laser for pulse-on-demand range finders was also reported, where a small piece of a high-reflectivity (HR) coated bulk substrate of fused silica was manually assembled onto a resonantly driven micro-actuator [30].

This paper reports what is believed to be the first full demonstration of a wavelength tunable solid-state laser with simultaneous Q-switching, with both effects generated using a single MOEMS mirror, with only an introductory overview reported previously in [31]. The MOEMS mirror design with two-dimensional optical tilt control is characterized in section II. The novel concept of combined spectral and temporal tuning is described in the context of an end-pumped Yb:KGW laser in section III. The experimental characterization of a wavelength tunable CW Yb:KGW laser is then given in section IV, followed by characterization of the same wavelength tunable laser Q-switched in section V.

## II. MOEMS MIRROR WITH 2D TILT CONTROL

### *A. Design and fabrication*

To facilitate tunable laser wavelength and active laser Q-switching simultaneously, a MOEMS mirror with flexible, dual-axis movement capability was required. An electrothermal actuator exhibiting both static and resonant displacement schemes [32] was used with a circular mirror aperture to form the MOEMS mirror device. A commercial, multi-user silicon-on-insulator process by MEMSCAP Inc. (SOIMUMPs) was used to fabricate the MOEMS mirror. In brief, a patterned device layer of 10 µm-thick phosphorous-doped single crystal silicon (SCS) is released from a 400 µm-thick silicon substrate and a thin insulating layer of $SiO_2$ via a series of masked etch steps. The released SCS structure forms the mechanically functional parts that constitute the MOEMS device. An extensive characterization of the process was reported by Miller *et al.* [33] and by MEMSCAP Inc. themselves [34].

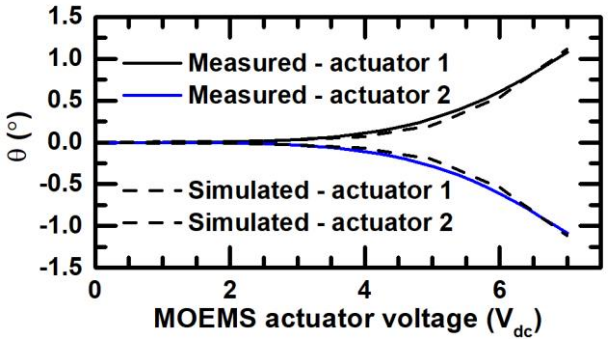


Figure 2: Measured and simulated optical mirror tilt angle, θ, about the mirror rest position with voltage applied separately to A1 and A2.

The actuator geometry, shown in Fig. 1(b), relied on three connected longitudinal beams each with a width of 40 µm, a length of 1800 µm and a center-to-center spacing of 175 µm. The three beams were anchored to the substrate independently at one end and were commonly connected to a released beam with a width of 80 µm and a length of 390 µm at the opposite end. The actuator was activated by supplying current flow through the outermost longitudinal beams, while no current flowed through the central longitudinal beam. Thermal expansion induced by Joule heating in the outer longitudinal beams and a mechanical constraint induced by the central longitudinal beam forced an out-of-plane displacement of the actuator.

In our design, four identical actuators, labelled A1-A4 in Fig. 1(b), were microfabricated radially around a released mirror aperture of 1.4 mm diameter and connected to it via serpentine suspension springs. A scanning electron microscope image of the fabricated MOEMS mirror is shown in Fig. 1(a). Vertical displacement of an actuator tip was translated to mirror tilt, with two-dimensional control enabled by the multi-actuator design. To render the mirror compatible for use in a laser system, a post-fabrication gold coating was deposited only on the mirror aperture, see Fig 1(b), using thermal evaporation. The gold layer had a thickness of 200 nm and yielded a reflectivity, R, of 96 % at $\lambda \approx 1$ µm. Stresses introduced by the fabrication process and by the deposition of the gold coating through the bimorph effect resulted in a concave MOEMS mirror surface curvature. The surface curvature was parabolic with a measured radius of curvature (ROC) of 50 mm near the center of the mirror.

The mirror tilt mechanism is shown in Fig. 1(c), taken from a finite element model built using COMSOL Multiphysics. The simulated optical tilt angle of the MOEMS mirror as a function of voltage applied to actuators 1 and 2 independently is shown in Fig. 2 and increases non-linearly to 1.14 ° in either direction from the mirror rest position at a voltage of 7 V. The maximum voltage that the actuator could withstand was simulated to be approximately 15 V, limited by the heat

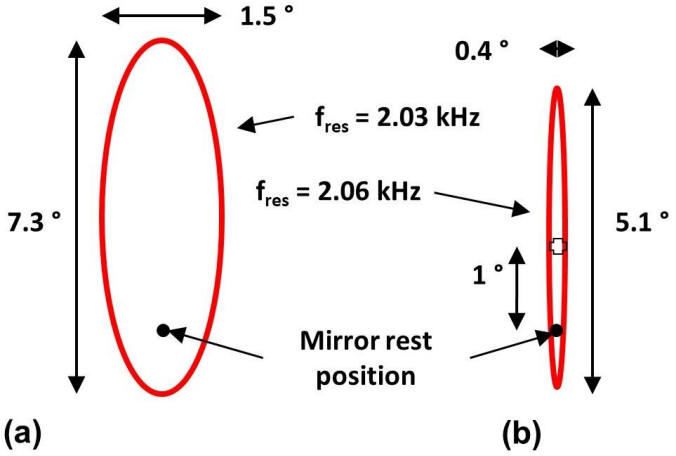


Figure 3: Diagram of the resonant mirror tilt movement as observed on a screen, (a) for 2.03 kHz applied to actuator A4, and (b) for 2.06 kHz applied to actuator A4.

dissipated in the MOEMS structure. The simulated optical tilt angle was 3.43 ° for this voltage, however for this laser application only tilt angles << 1 ° were required.

### *B. Static mirror tilt for laser wavelength tuning*

Static tilt of the MOEMS mirror was achieved by applying a DC voltage to one or more of the electrothermal actuators. The beam from a HeNe laser was directed towards the mirror surface and reflected onto a screen to analyse the mirror movement. Each actuator was assessed individually and showed a difference of less than 1 % in mirror tilt for the same voltage signal, albeit in different directions about the mirror rest position. Fig. 2 shows the measured optical tilt angle around the mirror rest position, achieved by applying a DC voltage (separately) to A1 and A2. Mirror tilt was instigated from 2 $V_{dc}$ and rose non-linearly to an optical tilt angle of 1.08 ° in either direction from the rest position for a voltage of 7 $V_{dc}$, with a switching time of 5 ms. The experimental results yielded a strong overlap with the FEM simulation, as shown in Fig. 2. These actuators, using this static tilt mechanism, were used to perform laser wavelength tuning as will be described in section III.

### *C. Resonant mirror tilt for laser Q-switching*

A different mode of MOEMS mirror tilt in the form of resonant scanning could be achieved by synchronising the drive signal frequency with an eigenfrequency of the MOEMS mirror. The tilt-mode eigenfrequency was simulated in COMSOL to be 1.97 kHz. The dynamic scanning movement was assessed using the same HeNe laser and screen setup. A square-wave voltage signal with a peak-to-peak amplitude of 10 V, offset of +5 V and duty cycle of 50 % was applied to actuator A4. A square-wave voltage signal was used to optimise the electrical to kinetic energy conversion. The tilt eigenfrequency mode of the addressed rotation axis was optimally excited at a frequency of 2.03 kHz, yielding a good overlap with the FEM simulation.

The multi-actuator design with identical actuators orientated on orthogonal axes led to inter-axis crosstalk, where actuating one axis resulted in a small response also being generated from the orthogonal axis. The crosstalk led to a non-linear scan pattern observed on the screen as shown in Fig. 3. An elliptical scan pattern was observed, with a measured optical scan angle of 7.3 ° along the major axis. The measured scan angle on the minor axis was 1.5 °. It was anticipated that the offset between the mirror rest position and the scan pattern on the minor axis would complicate alignment of the Q-switched laser. The mirror was consequently driven slightly off-resonance at $f_{res}$ = 2.06 kHz, leading to a smaller minor axis scan angle of 0.4 ° whilst resulting in an optical scan angle of 5.1 ° on the major axis. The centre point of the elliptical scan pattern was measured to be offset by 1 ° from the mirror rest position along the major axis.

## III. LASER DESIGN

### *A. Gain medium and end-pump configuration*

A 10 mm long, $N_g$-cut Yb:KGW crystal from Altechna was used as the laser gain medium for this proof-of-concept demonstration. This crystal can theoretically support laser wavelengths, $\lambda_{laser}$, between 1020 nm and 1060 nm when optically pumped at $\lambda_{pump}$ = 980 nm. The 5x2 mm end facets were anti-reflectance (AR) coated for $\lambda_{laser}$ and $\lambda_{pump}$. A custom-built copper block was used to mount the crystal, with openings at the end facets to allow beam propagation and a parallel channel for active water cooling at a constant temperature of 22 °C. Indium foil was used to enhance the thermal interface between the laser crystal and the copper block.

The Yb:KGW crystal was end-pumped by a fiber-coupled diode laser emitting at $\lambda_{pump}$ = 980 nm with a full width half maximum (FWHM) linewidth of 3.5 nm (LIMO35-F100-DL980-S1775, 100 µm core diameter, NA = 0.22). The diode laser was mounted on an air-cooling module maintained at 28 °C. The pump laser threshold was achieved at an input current of 6.3 A, and the pump laser output power, $P_{pump}$, rose linearly to 25.3 W for an input current of 40 A (see Fig. 4(a)).

To enhance the conversion efficiency of the Yb:KGW laser, the fiber-coupled pump beam was focused using a pair of plano-convex lenses labelled $L_1$ and $L_2$ with focal lengths 20 mm and 40 mm respectively in Fig. 4(b). The focused beam matched the fundamental mode size within the gain medium of a short two-mirror resonator, built up of M1 and M2 and used for beam alignment. The resonator included a high-reflective end-mirror (M1, R > 99.5%) with a ROC = 250 mm, the Yb:KGW crystal and a flat output coupler (OC) M2 with R = 80 % at $\lambda_{laser}$. M1 was positioned 8 mm from the pump-facing facet of the crystal and M2 was positioned 11 mm from the opposite crystal facet, resulting in cavity length of 29 mm. The curved end-mirror M1 contributed to focusing of the pump beam and was AR-coated for $\lambda_{pump}$ and HR-coated for $\lambda_{laser}$. A curved mirror was chosen at this position to allow convenient alignment of the tunable laser by using the short two-mirror laser with a flat OC as an alignment guide.

The ABCD-matrix simulated beam radius of the Yb:KGW laser at the center of the crystal was 146 µm, using a thermal lens estimation of 500 mm focal length at the center of the crystal. The pump beam radius, measured using a slit scanning beam profiler (Thorlabs BP109), varied between 110 µm and

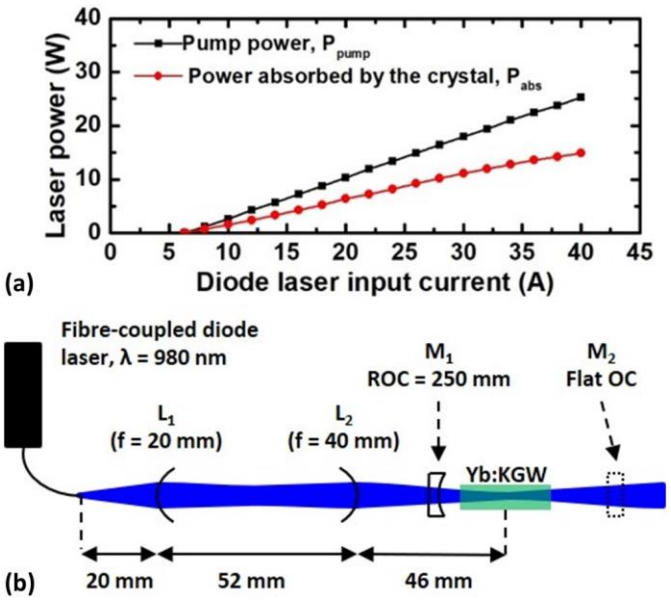


Figure 4: (a) Plot of pump diode laser input current against pump laser output power, $P_{pump}$, and the laser power absorbed by the Yb:KGW crystal, $P_{abs}$, (b) diagram of the end-pump setup with two lenses for beam focusing, the Yb:KGW crystal and a two-mirror cavity user for alignment of the laser shown in Fig. 5.

150 µm as the pump power increased from 2.7 W to 25 W, inherent of a change in $M^2$ beam quality factor from 23 to 30 on both the x- and y-axes. A top-hat transverse mode profile was measured throughout.

The pump power absorbed within the Yb:KGW crystal, $P_{abs}$, was calculated by taking the ratio of the pump power immediately before and after the crystal. Scattering from the lens surfaces L1 and L2 and the laser end-mirror M1 resulted in losses of 5 % for the pump beam. 63 ± 2 % of the pump light was then absorbed by the crystal, leading to a maximum of $P_{abs}$ = 14.9 W (see Fig. 4(a)). A tail-off was observed at abrosbed pump powers exceeding 13.2 W, indicating the onset of thermal influence on the Yb:KGW crystal. The absorbed pump power was consequently limited to 13.2 W in this work. The two-mirror laser was constructed and yielded a laser threshold condition of $P_{abs}$ = 9.7 W, a maximum output power of 1.4 W at $P_{abs}$ = 13.2 W, and a slope efficiency of 40 %.

### *B. Laser functionality overview*

The Littman-Metcalf configuration [13-15] was adopted for this work and modified for compatibility with a fully intracavity Yb:KGW laser. An equilateral SF11 prism with 20 mm side length was used for wavelength dispersion while the tilt angle of the MOEMS mirror determined the oscillating wavelength. The prism replaced the diffraction grating used in the original Littman-Metcalf configuration to yield intracavity losses of < 1 % when orientated close to the Brewster angle, with the laser oscillation linear polarized in the plane shown in Fig. 5.

A three-mirror resonator was built around the crystal as shown in Fig. 5. The 548 mm-long cavity was designed using ABCD-matrix evaluation to achieve a beam radius of 140 µm within the Yb:KGW crystal, matching the radius of the pump beam, and also to yield a spot radius of 75 µm on the MOEMS mirror. A thermal lens of 500 mm focal length was assumed,

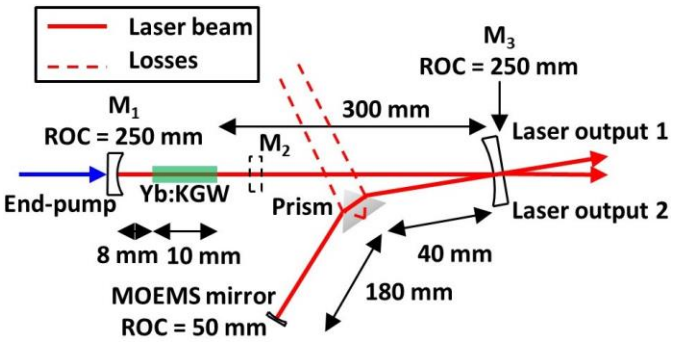


Figure 5: Diagram of the three-mirror laser configuration incorporating a Yb:KGW crystal, a SF11 equilateral prism for wavelength dispersion and the electrothermally actuated MOEMS mirror to actively tune the spectral and temporal laser output characteristics. Mirror $M_1$ was AR-coated for $\lambda_{pump}$ and HR-coated for $\lambda_{laser}$. $M_2$ was the OC from the alignment laser shown in Fig. 4. $M_3$ was both a folding mirror and the cavity OC with R = 98 % at $\lambda_{laser}$.

however a focal length value between 200 mm and infinity showed a beam radius variation < 1 % within the crystal. On the pump-facing side, the end-mirror M1 from section III-A was maintained. A folding mirror M3 with ROC = 250 mm and R = 98 % at $\lambda_{laser}$ was introduced into the laser cavity and also served as the OC for the tunable laser. This mirror was positioned 300 mm from the opposite crystal facet. M3 focused the beam through the prism and onto the MOEMS mirror, which had a ROC = 50 mm. The original Littman-Metcalf configuration used the first order diffraction mode of the grating as the laser output beam, while the partially transmissive folding mirror M3 facilitated the output in this work, leading to two output beams labelled laser output 1 and laser output 2 in Fig. 5 through the L-shaped laser cavity.

The prism and MOEMS mirror were orientated such that tilting the MOEMS mirror on the in-plane laser axis selected the oscillating wavelength. The orthogonal laser axis was therefore available for further laser functionality. Consequently, active Q-switching by resonantly scanning the mirror through laser alignment was possible simultaneously to wavelength tuning. A1 and A2 are, in this work, actuated using the static mirror tilt mechanism to achieve laser wavelength tuning, whilst A4 is actuated using the resonant mirror tilt mechanism to achieve laser Q-switching. Actuation of A4 thereby selected if the laser was CW or Q-switched. A3 was unused in this work.

### *C. Measurement setup*

In the laser cavity configuration used, two output beams with identical power were transmitted by M3 due to a double-pass transit made during a single round trip of the cavity (see Fig. 5). One of the beams was used to measure the spectral characteristics of the laser output, whilst the other was used to measure the temporal characteristics. An optical spectrum analyzer (OSA, HP86142A) with a resolution bandwidth of 0.1 nm and a video bandwidth of 2 kHz was used to measure the spectral characteristics. A FP/APC fiber optic collimator and patch cable were used to couple the beam into the OSA for measurement. A high-pass edge filter with a cut-off wavelength of 1 µm was used prior to patching to filter out the

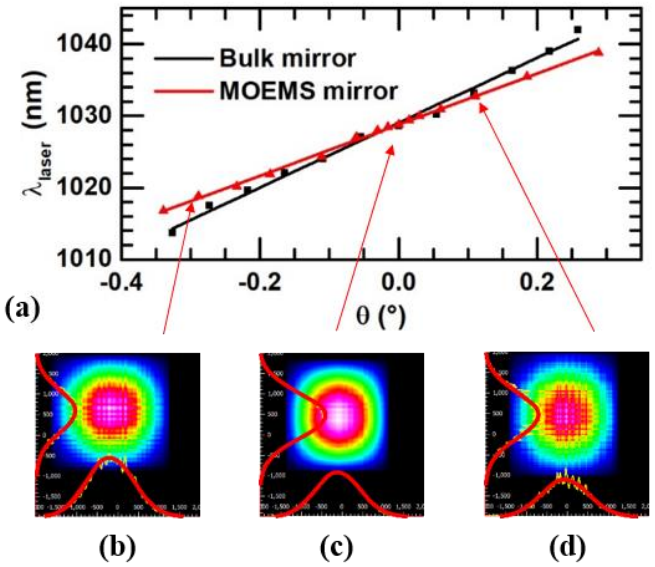


Figure 6: (a) Plot showing change in laser wavelength against mirror tilt angle for the MOEMS mirror and the bulk mirror, and the transverse mode profile of the laser output measured at MOEMS mirror tilt angles of (b) – 0.29 °, (c) 0 ° and (d) 0.11 °. All measurements were taken at a laser output power of 5 mW.

residual pump light. The temporal characteristics of the laser were measured by focusing the second output beam onto a fast photodiode (1.5 GHz) connected via an amplifier to an oscilloscope. The spatial properties of the laser output were measured separately by inserting a CCD camera (DataRay WinCamD-UC012-1310) or a slit scanning beam profiler (Thorlabs BP109) into the output beam path. The transverse mode profile was measured directly and the $M^2$ beam quality factor was measured by inserting a lens with 100 mm focal length prior to the CCD camera and measuring the beam width in 10 mm intervals up to 70 mm from the beam waist.

## IV. Tunable CW Yb:KGW Laser

The laser shown in Fig. 5 was aligned with the MOEMS mirror at its rest position. The CW laser threshold was reached at $P_{abs}$ = 7.8 W, leading to a peak center wavelength of $\lambda_0$ = 1028.5 nm and a FWHM linewidth of 0.3 nm, measured using the OSA. To prevent thermal damage to the surface of the MOEMS mirror, resulting from residual absorption within the reflective gold layer, the CW laser output power from a single output beam was limited to 5 mW for this experiment. A linear relationship between laser wavelength and mirror tilt angle was observed, as shown in Fig 6. A DC voltage applied to actuator A1 yielded a positive tilt angle (counter clockwise rotation), while a DC voltage applied to actuator A2 yielded a negative tilt angle (clockwise rotation). The wavelength decreased to 1016.8 nm with 5.2 V (θ = -0.34 °) applied to A2 and increased to 1038.8 nm with 5.0 V (θ = 0.29 °) applied to A1, equivalent to yielding 34.9 nm/°.

It was also observed that the laser threshold increased with increasing MOEMS mirror tilt angle in both directions from the center wavelength position (see Fig. 7). This was due to the non-uniform gain cross section of Yb:KGW [34] over the addressed wavelength range. The range of laser wavelengths

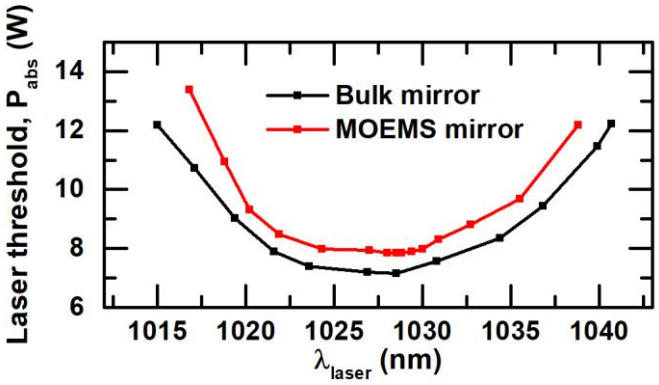


Figure 7: Plot showing absorbed pump power, $P_{abs}$, to reach laser threshold as the wavelength was tuned by the MOEMS mirror.

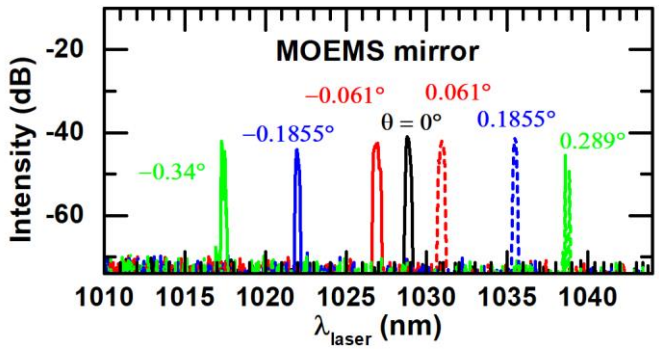


Figure 8: Plot showing the optical spectrum of the laser output for a range of MOEMS mirror tilt angles.

achieved was thereby limited by the set limit of $P_{abs}$ = 13.2 W and the gain curve of the Yb:KGW crystal.

The FWHM linewidth of each selected laser wavelength was measured to be below 0.3 nm. Sample optical spectra of the laser output are shown in Fig. 8 for different mirror tilt angles. A beam quality factor of $M^2 < 1.1$ was measured at the center and extreme laser wavelengths and a $TEM_{00}$ transverse mode profile was measured at the same positions using the slit scanning beam profiler, as shown in Fig. 6 (b)-(d). No discernable change in linewidth, $M^2$ or transverse mode profile was observed between laser threshold and an output power of 5 mW. The absorbed pump power to achieve an output power of 5 mW was observed to be less than 0.1 W higher than the laser threshold condition throughout.

The performance of the MOEMS mirror in the laser was further evaluated by comparing the wavelength tuning results to that of a similar cavity where the MOEMS was replaced by a standard 1" diameter BK7 mirror, with a ROC of 50 mm and R = 98 % at $\lambda_{laser}$. The tilt angle of the mirror was adjusted using the manual tip-tilt mechanism of a standard commercial (Newport) mirror mount. Similar wavelength tuning characteristics to that measured during use of the MOEMS mirror configuration were obtained. A linear relationship was observed, yielding 48.0 nm/° between laser wavelengths of 1013.7 nm (θ = - 0.33 °) and 1042.0 nm (θ = 0.26 °) as shown in Fig. 6(a). The difference in slope was assumed to be due to heat-induced curvature change of the MOEMS mirror, the effects of which are discussed in section VI. The wavelength range was again limited by the set limit of 13.2 W applied to $P_{abs}$. A lower laser threshold (see Fig. 7) was achieved due to

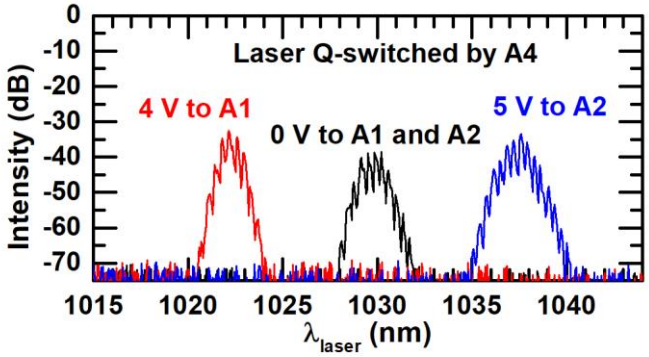


Figure 9: Optical spectrum of the Q-switched laser output for the center and extreme laser wavelengths, taken using the OSA.

the difference in reflectivity between the MOEMS mirror and the bulk mirror, resulting in a higher achievable range of laser wavelengths.

## V. Tunable, Q-switched Yb:KGW laser

In this section the simultaneous Q-switching and wavelength tuning of a laser output using the single MOEMS mirror of the previous sections is described. This required that two orthogonal actuators in the MOEMS device were electrically driven with separate driving signals. This, to the best of our knowledge, is the first demonstration of such a concept, where a single MOEMS mirror controls two output characteristics of the Yb:KGW laser. The CW laser described in the previous section was aligned initially at the MOEMS mirror rest position, producing an output at 1028.5 nm. While actuators A1 and A2 were maintained under no actuation, a 2.06 kHz voltage signal with an amplitude of 10 V, offset of +5 V and a duty cycle of 50 % was then applied to the orthogonal actuator A4. The minor axis offset of the non-linear resonant movement of the mirror, shown previously in Fig. 3, resulted in a misalignment of the laser. The laser was subsequently re-aligned manually on the in-plane laser axis such that the adjacent left-hand edge of the scan movement coincided with the initial mirror rest position.

The Q-switched laser threshold was reached at $P_{abs}$ = 8.7 W. To prevent ablation of the MOEMS mirror surface, the average laser output power was limited to 5 mW for this investigation. The center wavelength was measured to be $\lambda_0$ = 1029.6 nm with a FWHM linewidth of 1.1 nm using the OSA, as shown in Fig. 9. The laser exhibited a Q-switch pulse repetition rate of 2.06 kHz, equivalent to one output pulse per MOEMS movement cycle. A sample of the laser output pulse train is shown in Fig. 10(a), measured using the fast photodiode and the oscilloscope. An average pulse duration of 700 ns (see Fig. 10(b)), timing jitter of 40 ns and amplitude jitter of ~25 % were measured, assumed to originate from operation close to laser threshold. A $TEM_{00}$ transverse mode profile was observed using the CCD camera, shown in Fig. 11(b)-(d), and the $M^2$ was measured to be less than 1.05.

Whilst the laser was operating in Q-switch mode, simultaneous static tilt of the mirror on the in-plane laser axis was then initiated by supplying a DC voltage to actuator A1 or A2. The optical mirror tilt angle, θ, was measured between the mirror rest position and the adjacent crossing of the tilted scan

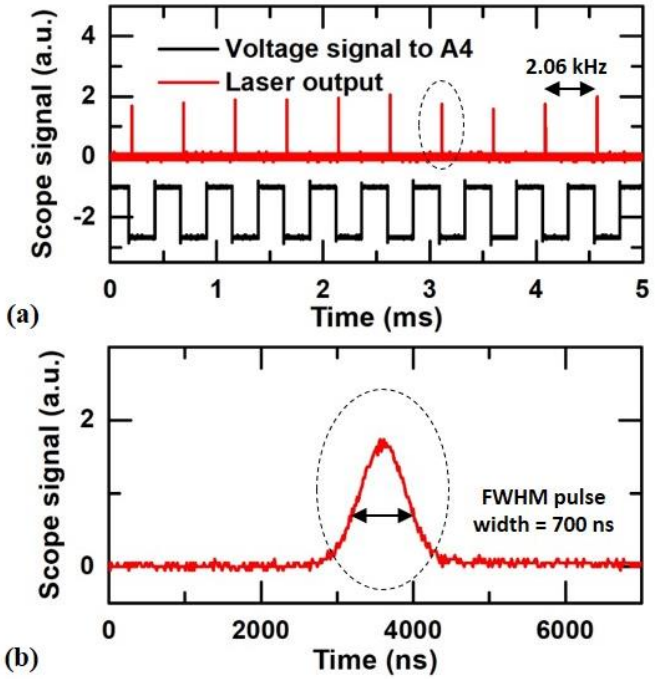


Figure 10: (a) Temporal plot showing a sample laser output pulse train and its relation to the voltage signal applied to A4, and (b) a sample pulse illustrating a FWHM pulse width of 700 ns.

movement, and yielded a similar characteristic to that of the independent static mirror tilt mechanism described in section II-B.

The laser wavelength decreased to a minimum of 1022.2 nm (linewidth of 0.8 nm) with 4.0 $V_{dc}$ applied to A1, corresponding to an optical tilt angle of - 0.16 ° for the MOEMS mirror. A non-linearity was observed when tilting the MOEMS mirror in the opposite direction using A2, resulting from the non-linear resonant movement of the mirror. The laser wavelength increased to 1030.5 nm for 3.9 $V_{dc}$ applied to A2, as anticipated from prior experiments. However, the transition from 3.9 $V_{dc}$ to 4.0 $V_{dc}$ then caused a sudden shift in laser wavelength from 1030.5 nm to 1027.6 nm, shown in Fig. 11(a). This was due to the opposite right-side swing of the resonant mirror movement (see Fig. 3) tilting into laser alignment and yielding a higher gain than that of the left-side swing, which was previously in laser alignment. The laser wavelength then increased to a maximum of 1037.5 nm for 5.0 V applied to A2. The minimum and maximum laser wavelengths were limited by $P_{abs}$, where 13.2 W was required to reach 5 mW average output power.

Q-switch pulse durations ranging between 460 ns and 740 ns were measured between the shortest and longest addressed laser wavelengths. The variation arose from the effects of the wavelength tuning on the laser dynamics and the dependency of the pulse duration on the cavity gain [28], which was altered from measurement to measurement. A $TEM_{00}$ transverse mode profile was measured at the center, upper and lower laser wavelengths and the maximum measured $M^2$ was 1.05.

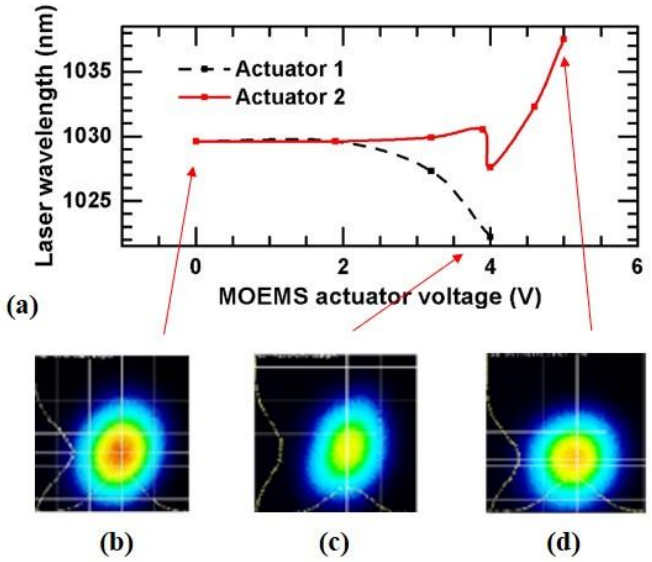


Figure 11: (a) Plot showing change in laser wavelength against mirror tilt angle for the MOEMS mirror whilst Q-switching, and the transverse mode profile of the laser output measured at voltages of (b) 0 V applied to actuators A1 and A2, (c) 4.0 V applied to actuator A1 and (d) 5.0 V applied to actuator A2. All measurements were taken at an average laser output power of 5 mW.

## VI. Discussion

The laser output power in this work was intentionally limited to 5 mW average power to avoid thermal failure of the MOEMS device in both CW and Q-switched operation. The R = 96 % yielded by the gold coating results in a significant amount of absorption and heating of the material layers, inherently causing curvature changes from the bimorph effect or even hole burning on the mirror surface. This could be circumvented with the deposition of a robust, HR dielectric multi-layer coating. However, just like the previously reported use of intracavity MOEMS mirrors in solid-state lasers [27-29], challenges remain in obtaining a repeatable flat MOEMS mirror surface (low-stress) with athermal curvature and R > 99 %. Through this, the power-scaling of MOEMS-based solid-state lasers poses an important challenge when aimed towards manufacturing and military-grade laser systems. In such cases, and in the case of dielectric coatings, absorption within the silicon layer of the MOEMS can also be reduced when operating at $\lambda > 1500$ nm.

The use of a prism as dispersing element compared to the more commonly used diffraction grating was necessary to minimize the intracavity losses of the laser. Whilst most blazed gratings can yield a first-order diffraction mode efficiency in the range of 60% - 90%, such losses would have an adverse impact on the laser conversion efficiency. With the coated MOEMS mirrors adding a further 4% loss to the cavity, the lower loss case of the prism orientated near the Brewster angle was preferred in this work. The spectrum dispersed by the prism resulted in the laser beam spot shifting across the MOEMS mirror surface. Using a MATLAB script, it was calculated that laser wavelengths between 978 nm and 1085 nm occurred fully within the confines of the MOEMS mirror aperture, assuming a central wavelength of 1028.5 nm and a beam spot radius of 75 µm. If a laser gain medium yielding a larger gain bandwidth is to be used, the spectrum incident on the MOEMS mirror must be considered.

The curved surface of the MOEMS mirror also had an impact on the tunable laser characteristics. The curved mirror surface influenced the directionality of the reflected spectrum, and in fact reversed the expected direction of mirror tilt to decrease or increase the laser wavelength in this case. This was due to the prism being located further than the focal point of the mirror, resulting in a crossing point for the laser wavelengths at the extremes of the gain bandwidth. It was possible that, if the prism was located at the mirror focal point, all laser wavelengths would be in laser alignment simultaneously. In such a case, the wavelength of highest gain would dominate, and wavelength tunability would not be achievable. A flat mirror surface would reverse the mirror tilt required to decrease and increase the laser wavelength and eliminate cavity design complications.

The CW wavelength tuning showed no discernable mode-hopping, which allowed continuous addressing of the wavelength range supported by the gain medium. In Q-switched operation, the observed spiking of the output linewidth (see Fig. 9) is assumed to be associated with convolution between the OSA sweep time and the Q-switch pulses, but still yields a continuously tunable output. A widening of the Q-switched laser linewidth was also observed, expected to be a result of the high energy density within the crystal and rapid release inherent of Q-switch operation.

The laser dynamics of the Q-switched output show pulse durations which are potentially limited by the mirror movement speed through the cavity alignment [28]. With a mirror designed for higher angular speed (e.g. by piezoelectric actuation), the potential to allow cavity-limited pulse durations in future work is possible. Longer pulse durations were also possible by reducing the amplitude of the voltage signal applied to actuator A4. The major axis scan angle and movement speed of the MEMS mirror were thereby reduced, elongating the gate time for pulse emission. Furthermore, with an improved mirror design, a linear resonant scanning movement would enable two Q-switch pulses per MOEMS movement cycle and mitigate the laser alignment issues described in section V.

Further flexibility could also be added to the laser through tunable Q-switch repetition rate, which could be achieved by tuning the driving signal frequency of the MOEMS actuator. This would be limited by the resonant operating range of the MOEMS mirror and would inherently affect the pulse duration, since the optical scan angle would be reduced by driving the MOEMS mirror off-resonance. Furthermore, with the Q-switch repetition rate directly controlled by the resonant frequency of the MOEMS mirror, the MOEMS design has a direct impact on laser performance. The optimized actuator design could be used with a mirror aperture of suitable diameter to achieve the desired resonant frequency and hence Q-switch repetition rate.

The proof-of-concept demonstration in this work shows nevertheless the applicability of the MOEMS control technique, with current on-going work of mirror performance enhancements having the potential to further improve the mentioned points.

## VII. Conclusion

In this work, we have presented the first wavelength tunable solid-state laser enabled by an intracavity MOEMS mirror. Further flexibility was then added in the form of simultaneous laser wavelength tuning and Q-switching using the same MOEMS mirror. A continuous tuning range of 22 nm was achieved under CW laser operation for an end-pumped Yb:KGW laser, and a range of 15.3 nm was achieved for the same laser under Q-switched operation. The achieved wavelength range was limited by cavity losses. A pulse repetition rate of 2.06 kHz was obtained with pulse widths varying between 460 ns and 740 ns across the range of laser wavelengths. The reported technique can be directly applicable in the 2µm range or in the mid-infrared by using appropriate gain media and coatings on the bulk laser cavity optics. Full digital control of the laser output wavelength over the crystal gain bandwidth, combined with Q-switched output on demand, allows this to be a promising step towards a fully digital configurable solid-state laser with full temporal, spectral and spatial control.

## VIII. Acknowledgement

The authors would like to thank Dr J. Mackersie for depositing the post-fabrication gold coatings on the MOEMS mirror and Dr R. Li for his assistance in the initial setup of the end-pump system for the Yb:KGW laser.

## IX. References

[1] S. Holmstrom, U. Baran and H. Urey, "MEMS laser scanners: a review," *Journal of Microelectromechanical Systems*, Vol. 23 (2), pp. 259-275, Apr. 2014.

[2] K. Ikegami, T. Koyama, T. Saito, Y. Yasuda and H. Toshiyoshi, "A biaxial piezoelectric MEMS scanning mirror and its application to pico-projectors," *2014 International Conference on Optical MEMS and Nanophotonics*, Glasgow, UK, 2014, pp. 95-96.

[3] A. Wolter, H. Schenk, E. Gaumont and H. Lakner, "MEMS microscanning mirror for barcode reading: from development to production," *MOEMS Display and Imaging Systems II*, Proc. SPIE 5348, San Jose, CA, Jan. 2004.

[4] D. Dickensheets and G. Kino, "Micromachined scanning confocal optical microscope," *Optics Letters*, Vol. 21 (10), pp. 764-766, May 2016.

[5] W. Piyawattanametha, "3-D near-infrared fluorescence imaging using a MEMS-based miniature dual-axis confocal microscope," *IEEE Journal of Selected Topics in Quantum Electronics*, Vol. 15 (5), pp. 1344-1350, Sep. 2009.

[6] R. Bauer and D. Uttamchandani, "MEMS micromirror based light sheet generator for biomedical imaging," *2017 International Conference on Optical MEMS and Nanophotonics*, Santa Fe, NM, USA, 2017, pp. 129-130.

[7] R. Li, M. Griffith, L. Laycock and W. Lubeigt, "Controllable continuous-wave Nd:$YVO_4$ self-Raman lasers using intracavity adaptive optics," *Optics Letters*, Vol. 39 (16), pp. 4762-4765, Aug. 2014.

[8] M. Lackner *et al*., "CO and $CO_2$ spectroscopy using a 60 nm broadband tunable MEMS-VCSEL at ~ 1.55 µm," *Optics Letters*, Vol. 31 (21), pp. 3170-3172, Nov. 2006.

[9] V. Jayaraman, G.D. Cole, M. Robertson, A. Uddin, and A. Cable, "High-sweep-rate 1310 nm MEMS-VCSEL with 150 nm continuous tuning range," *Electronics Letters*, Vol. 48 (14), pp. 867-869, July 2012.

[10] E.C. Vail, M.S. Wu, G.S. Li, L.E. Eng and C.J. Chang-Hasnain, "GaAs micromachined widely tunable Fabry-Perot filters," *Electronics Letters*, Vol 31 (3), pp. 228-229, Feb.1995.

[11] C.J. Chang-Hasnain, "Tunable VCSEL," *IEEE Journal on Selected Topics in Quantum Electronics*, Vol. 6 (6), pp. 978-987, Nov. 2000.

[12] A.Q. Liu and X.M. Zhang, "A review of MEMS external-cavity tunable lasers," *Journal of Micromechanics and Microengineering*, Vol. 17 (1), pp. R1, Jan. 2007.

[13] M.G. Littman and H.J. Metcalf, "Spectrally narrow pulsed dye laser without beam expander," *Applied Optics*, Vol. 17 (14), pp. 2224-2227, 1978.

[14] M.G. Littman, "Single-mode operation of grazing-incidence pulsed dye laser," *Optics Letters*, Vol. 3 (4), pp. 138-140, 1978.

[15] K. Liu and M.G. Littman, "Novel geometry for single-mode scanning of tunable lasers," *Optics Letters*, Vol. 6 (3), pp. 117-118, 1981.

[16] W. Huang, R.R.A. Syms, J. Stagg and A. Lohmann, "Precision MEMS flexure mount for a Littman tunable external cavity laser," *Science, Measurement and Technology*, IEEE Proc. Vol. 151 (2), pp. 67-75, Mar. 2004.

[17] A. Inoue, T. Komikado, K. Konishita, J. Hayashi and S. Umegaki, "Deformable Mirror for Mechanical Q-switching of Laser-Diode-Pumped Microchip Laser," *Japanese Journal of Applied Physics*, Vol. 46 (42), pp. L1016-L1018, Oct. 2007.

[18] J. Masson, R. St-Gelais, A. Poulin and Y. Peter, "Tunable Fiber Laser Using a MEMS-Based In Plane Fabry-Perot Filter," *IEEE Journal of Quantum Electronics*, Vol. 46 (9), pp. 1313-1319, Sep. 2010.

[19] D. Michel, F. Xiao and K. Alameh, "MEMS-Based Tunable Linear-Cavity Fiber Laser," *IEEE Photonics Journal*, Vol. 4 (3), pp. 895-902, June 2012.

[20] Y. Peter, H.P. Herzig, E. Rochat, R. Daendliker, C. Marxer and N.F. de Rooij, "Pulsed fiber laser using micro-electro-mechanical mirrors," *Optical Engineering*, SPIE Vol. 38 (4), pp. 636-640, 1999.

[21] M. Fabert, A. Desfarges-Berthelemot, V. Kermene, A. Crunteanu, D. Bouyge and P. Blondy, "Ytterbium-doped fibre laser Q-switched by a cantilever-type micro-mirror," *Optics Express*, Vol. 16 (26), pp. 22064-22071, 2008.

[22] M. Fabert, A. Desfarges-Berthelemot, V. Kermene and A. Crunteanu, "Temporal synchronization and spectral combining of pulses from fiber lasers Q-switched by independent MEMS micro-mirrors," *Optics Express*, Vol. 20 (20), pp. 22895-22901, Sep. 2012

[23] V. Couderc, A. Crunteanu, M. Fabert, F. Foutre, F. El Bassri, D. Pagnoux and A. Jalocha, "Picosecond pulse generation in a hybrid Q-switched laser source by using a microelectromechanical mirror," *Optics Express*, Vol. 20 (5), pp. 5524-5529, Feb. 2012.

[24] A. Crunteanu, D. Bouyge, D. Sabourdy, P. Blondy, V. Couderc, L. Grossard, P.H. Pioger and A. Barthelemy, "Deformable micro-electro-mechanical mirror integration in a fibre laser Q-switch system," *Journal of Optics A: Pure and Applied Optics*, Vol. 8 (7), pp. 347-351, 2006.

[25] D. Bouyge, A. Crunteanu, V. Couderc, D. Sabourdy and P. Blondy, "Synchronized tunable Q-switched fiber lasers using deformable achromatic microelectromechanical mirror," *IEEE Photonics Technology Letters*, Vol. 20 (12), pp. 991-993, June 2008.

[26] M. Fabert, V. Kermene, A. Desfarges-Berthelemot, P. Blondy and A. Crunteanu, "Actively mode-locked fiber laser using a deformable micromirror," *Optics Letters*, Vol. 36 (12), pp. 2191-2193, June 2011.

[27] W. Lubeigt, J. Gomes, G. Brown, A. Kelly, V. Savitski, D. Uttamchandani and D. Burns, *Optics Express*, Vol. 19 (3), pp. 2456-2465, Jan. 2011.

[28] R. Bauer, A. Paterson, C. Clark, D. Uttamchandani and W. Lubeigt, "Output Characteristics of Q-switched Solid-State Lasers Using Intracavity MEMS Micromirrors," IEEE Journal of Selected Topics in Quantum Electronics, Vol. 21 (1), pp. 356-363, Jan. 2015.

[29] R. Bauer, W. Lubeigt and D. Uttamchandani, "Dual Q-switched laser outputs from a single lasing medium using an intracavity MEMS micromirror array," *Optics Letters*, Vol. 37 (17), pp. 3567-3569, Aug. 2012.

[30] V. Milanovic *et al*., "Compact MEMS mirror based Q-switch module for pulse-on-demand laser range finders" *Photonics West*, SPIE Proc. Vol. 9375, pp. 93750H, Feb. 2015.

[31] A. Paterson, R. Bauer, W. Lubeigt, and D. Uttamchandani, "Q-switched tunable solid-state laser using a MOEMS mirror" *2017 International Conference on Optical MEMS and Nanophotonics*, Santa Fe, NM, USA, 2017, pp. 27–28.

[32] L. Li and D. Uttamchandani, "Dynamic response modelling and

characterization of a vertical electrothermal actuator," *Journal of Micromechanics and Microengineering*, Vol. 19 (7), pp. 0750134, June 2009.
[33] D.C. Miller, B.L. Boyce, M.T. Dugger, T.E. Buchheit and K. Gall, "Characteristics of a commercially available silicon-on-insulator MEMS material," *Sensors and Actuators A: Physical*, Vol. 138 (1), pp. 130-144, July 2007.
[34] A. Cowen, G. Hames, D. Monk, S. Wilcenski and B. Hardy, *SOIMUMPS Design Handbook*, Durham, NC: MEMSCAP Inc., Revision 8.0 ed. [Online]. Available http://www.memscap.com
[35] A.A. Lagatsky, N.V. Kuleshov and V.P. Mikhailov, "Diode-pumped CW Yb:KGW and Yb:KYW Minilasers," *Advanced Solid State Lasers*, Boston, MA, 1999, pp. TuB12.

**Alan Paterson** received the Meng degree in Electronic and Electrical Engineering from the University of Strathclyde, UK, in 2008. He is currently in the thesis write-up phase of his PhD degree at the same university, based on investigating the synergies between MOEMS and solid-state laser technology.

He is currently working for Sencio BV, the Netherlands, as a development engineer for customised packaging for MEMS and sensor technology.

**Ralf Bauer** (M'17) received the Dipl.-Ing. degree in Mechatronics from the University of Erlangen-Nuernberg, Germany in 2010, and the Ph.D. degree from the University of Strathclyde, Glasgow, U.K., in 2013 for work on MEMS solid-state lasers.

He is currently a Lecturer and RAEng Engineering for Development Research Fellow in the Centre for Microsystems and Photonics, University of Strathclyde, working on optical MEMS devices for laser systems and biomedical imaging applications. His research interests include the development and integration of MEMS in optical systems, miniaturized biomedical imaging systems and laser systems.

Dr Bauer is a member of the IEEE and Optical Society (OSA).

**Walter Lubeigt** received the Engineering Diploma degree in opto-electronic systems from the Ecole Supérieure des Procédés Electroniques et Optiques, University of Orléans, France in 2001. He then received the PhD. degree from the University of Strathclyde, Glasgow, U.K. in 2006 for work on solid-state laser performance enhancement using intracavity adaptive optics techniques.

He subsequently worked on the development of diamond Raman lasers at the Institute of Photonics, University of Strathclyde. In 2010, he joined the Centre for Microsystems and Photonics, University of Strathclyde, as a John Anderson Research Lecturer. His research interests included the development of MEMS-controlled solid-state lasers, the use of intracavity adaptive optics to improve the performance of solid-state Raman lasers and the development of novel laser systems for environmental remote sensing.

Dr Lubeigt currently works for M Squared lasers as a senior laser engineer.

**Deepak Uttamchandani** (SM'05) received the Ph.D. degree from University College London, London, U.K., in the area of optical fiber sensors, in 1985.

He is currently the Head of the Centre for Microsystems and Photonics, University of Strathclyde, Glasgow, U.K. His early research in MEMS concentrated on optothermal microresonator sensors and in investigating techniques for general MEMS material characterization using MEMS micromechanical resonators. His recent research has concentrated on system applications of optical MEMS including intracavity MEMS-based laser systems, MEMS-based directional microphones and MEMS-based single-pixel imaging systems. He has also published in the field of optical sensors including subwavelength tip-based Raman spectroscopy, which has contributed to the development of tip-enhanced Raman spectroscopy and in the area of *in situ* intraocular drug detection systems via optical spectroscopy in the living eye.